Warm Molecular Hydrogen in the Galactic Wind of M82[1]

Sylvain Veilleux[2,3], David S. N. Rupke[4], and Rob Swaters[2]

ABSTRACT

We report the detection of a complex of extraplanar warm-H_2 knots and filaments extending more than ∼3 kpc above and below the galactic plane of M82, roughly coincident with the well-known galactic wind in this system. Comparisons of these data with published results at other wavelengths provide quantitative constraints on the topology, excitation, heating, and stability against disruption of the wind-entrained molecular ISM in this prototypical galactic wind. Deep H_2 2.12 μm observations such as these represent a promising new method to study the elusive but potentially important molecular component of galactic winds.

Subject headings: galaxies: halos — galaxies: individual (M82) — galaxies: ISM — galaxies: starburst — ISM: jets and outflows — ISM: molecules

1. Introduction

Galaxy-scale outflows of gas ("superwinds") are a ubiquitous phenomenon in both starburst galaxies and those containing an active galactic nucleus (Veilleux et al. 2005). The observational data set on these outflows is steadily increasing, but difficult issues remain. One vexing problem is how much different phases of the ISM contribute to the mass and energy of superwinds. Measurements have shown that winds contain cool (molecular or neutral), warm (ionized) and hot (highly ionized) material. However, the relative contribution of

[2]Department of Astronomy, University of Maryland, College Park, MD 20742; veilleux@astro.umd.edu, swaters@astro.umd.edu

[3]Also: Max-Planck-Institut für extraterrestrische Physik, Postfach 1312, D-85741 Garching, Germany

[4]Institute for Astronomy, University of Hawaii, 2680 Woodlawn Drive, Honolulu, HI 96822; drupke@ifa.hawaii.edu

[1]This work is based on observations carried out with the facilities of NOAO. NOAO is operated by the Association of Universities for Research in Astronomy (AURA), Inc. under cooperative agreement with the National Science Foundation.

these phases to the total mass and energy of the wind is uncertain by an order of magnitude. The contribution from dust and molecular gas to the mass and energy in the wind is almost completely unknown. The impact of superwinds on their environments depends strongly on these quantities. Superwinds are invoked as enrichers of galactic halos and the IGM, but it is not yet clear if the winds extend far enough to carry dust, molecular gas, and metals out of the galaxy.

Some evidence already exists for outflowing dust in galaxy halos. A few winds have been mapped in the far-infrared (Hughes et al. 2004; Alton et al. 1999; Radovich et al. 2001), but these maps are of low resolution and sensitivity and only trace the coldest dust. In a few galaxies, large-scale, optically dark filaments are observed (Phillips 1993; Cecil et al. 2001; Howk 2009). UV observations have also revealed dust reflection in outflows in a few galaxies (Hoopes et al. 2005). Neutral gas is outflowing in most strong starbursts (Rupke et al. 2005a, 2005b) and extends over kpc scales in a few resolved galaxies (Rupke et al. 2005b; Martin 2006). As shown by extinction measurements, dust correlates with the neutral gas column in these galaxies, suggesting much of it is also outflowing (Veilleux et al. 1995). Finally, spectacular dust morphologies suggestive of large-scale winds have been detected in our Galaxy based on data from the Midcourse Space Experiment (MSX) satellite (Bland-Hawthorn & Cohen 2003) and in the prototypical outflow of M82 based on data obtained with *Spitzer*/IRAC (Engelbracht et al. 2006). To our knowledge, M82 is the only object among all galaxies with dusty winds with an unambiguously detected large-scale cold molecular outflow (Nakai et al. 1987; Loiseau et al. 1990; García-Burillo et al. 2001; Walter et al. 2002).

In this *Letter*, we present deep H_2 $v = 1{-}0$ S(1) 2.12 μm images of M82 that reveal a complex of warm H_2-emitting knots and filaments above and below the disk of M82, roughly coincident with the ionized and dusty components of the galactic wind in this object. The observations and methods of data reduction are briefly described in Section 2. In Section 3, the results are presented and compared with published data at other wavelengths. The implications of these results on the topology, excitation, heating, and stability of the wind-entrained material are discussed in Section 4. The main conclusions are summarized in Section 5. Throughout this paper, we assume a distance of 3.53 Mpc for M82 (Karachentsev et al. 2002).

2. Observations & Data Reduction

The NOAO Extremely Wide Field Infrared Mosaic (NEWFIRM; Probst et al. 2008 and references therein) on the Mayall 4-meter telescope at Kitt Peak was used for the observa-

tions. This instrument images a $28' \times 28'$ field of view with a 4K × 4K pixel InSb array mosaic on a $0\farcs4$ pixel scale. Total on-target integrations of 40 and 420 minutes were obtained over a period of four nights (1, 2, 4, and 5 November 2008 UT) using the broadband K_s and narrowband (1.1% resolution) H_2 2.124 μm filters, respectively. The so-called "4Q" observing mode of NEWFIRM was used for efficient acquisition of the data: M82 was placed near the center of one quadrant, and then it was cycled 10 (K_s) or 15 (H_2) times through each of the four quadrants, exposing at each position for 10 or 60 seconds, respectively, and applying random dither offsets within a box $30''$ on a side so that the positions did not exactly repeat from cycle to cycle. The number of frames coadded before being displayed was set to 6 at K_s and 1 at H_2, to improve the acquisition efficiency of the K_s observations. Per-pixel digital averaging of 4 and high-order Fowler sampling (Fowler & Gatley 1990) of 8 were used to reduce read noise in the H_2 data.

NOAO NEWFIRM Science Pipeline v1.0 was used to reduce these data (Swaters et al. 2009). After the data were dark-subtracted, linearized, and flat-fielded, a sky background image was determined for each exposure by taking the median of the four preceding and four subsequent exposures, but excluding exposures with the galaxy image in it. This sky image was then scaled to match the sky background in the galaxy exposures and subtracted. Astrometric solutions were obtained, and the data were resampled and stacked. Next, the sky subtraction was repeated, but while masking out objects detected in the first pass, and a new stack was produced. Persistent images, bad pixels, and transient effects were flagged and excluded in that stack.

3. Results

The continuum-subtracted H_2 image of M82 is shown in Figure 1. The stack of K_s images was used, after proper intensity scaling, to subtract off the continuum emission from the H_2 stack and produce the "pure" H_2 image presented in this figure. Immediately evident in Figure 1 are H_2 filaments extending more than ∼3 kpc above and below the plane of the galaxy disk, roughly coincident with the location of the galactic wind in M82 as traced by the warm ionized gas (e.g. Shopbell & Bland-Hawthorn 1998; Devine & Bally 1999; Lehnert et al. 1999; Westmoquette et al. 2009), the hot ionized gas (e.g. Lehnert et al. 1999; Strickland & Stevens 2000; Stevens et al. 2003; Strickland & Heckman 2009), the UV-scattering dust (Hoopes et al. 2005), and the cold molecular gas (Walter et al. 2002).

In Figures 2 and 3, our H_2 data are compared with the published Hα and 7.7 + 8.6 μm PAH images of Mutchler et al. (2007) and Engelbracht et al. (2006), respectively. The Hα data were continuum-subtracted using an optimal linear combination of the V- and I-band

data. In the bright central disk (middle panels in Figure 3), there appears to be large- and small-scale correspondence between the H_2 emission and the PAH morphology. Immediately outside this bright disk, the correspondence is weaker: radial streamers are seen in both images but their relative intensities differ with wavebands. None of these streamers exactly coincides with the shock-excited [Fe II] 1.64 μm and mm-wave SiO filaments detected by Alonso-Herrero et al. (2003) and García-Burillo et al. (2001), respectively.

On larger scales (top and bottom panels in Figure 3), the brightest H_2 structures are near bright PAH structures. The ratio of H_2 to PAH emission in the bright H_2 clumps shows a clear tendency to increase with distance from the nucleus (right panel in Figure 2), while at fainter flux levels (left panel in Figure 2) the PAH emission is overall more broadly distributed than the H_2 emission. This last result is not due to a lack of sensitivity at H_2. It reflects a true physical difference in the distribution of the warm H_2 gas relative to the faint PAH emission (see Section 4.2).

The Hα emission tends to extend in roughly the same directions as the H_2 and PAH emission, though the faint PAH and H_2 emissions are wider-angle. The SE extension is prominent at all three wavelengths, while the N-NE outflow is most prominent in Hα. The H_2 emission in the SE extension is also fairly well correlated with the "inverted" ionization cone seen in the [N II]/Hα ratio map of Shopbell & Bland-Hawthorn (1998; their figure 4). However, the match sometimes breaks down on smaller scale. The examples shown in Figure 4 are not necessarily representative, but they illustrate the complexity of the multi-phase material entrained in the wind (see Sections 4.1 and 4.2).

One last but important comparison is made with the distributions of the mm-wave CO emission from the cold molecular gas (Walter et al. 2002) and the dust-scattered UV halo seen in the *GALEX* data (Hoopes et al. 2005). Most of the features seen in CO are detected in H_2. The most prominent CO features are the central disk and the "streamers" that Walter et al. call S1-S4. Two of these, S1 and S2, are in the plane of the disk, and S1 at least is visible in H_2. S3 and S4 extend to the E-SE; S3 corresponds to the more easterly filament circled in the bottom panels of Figure 3. The CO emission in the other H_2 filaments to the SE is very faint, if at all present. As expected in photon-dominated regions (PDRs; Tielens & Hollenback 1985), the H_2 emission is more extended and probes clouds which are more diffuse (smaller A_V) and at larger distances from the nucleus than the CO emission. Deep H_2 2.12 μm observations are therefore a promising new method to study the molecular gas in galactic winds.

When combining all data sets, we find that the best multiwavelength match is found in the S-SE outflow cone. The UV emission does have the filamentary emission features seen in H_2 and Hα. In fact, two of the three prominent H_2 filaments appear well-correlated with the

UV. But, this is not true everywhere. The E-SE S3 CO streamer, which is fairly prominent in H_2, is not seen in UV or Hα – it appears to be obscured in the optical. And, in the NW region, CO is undetected, H_2 is faint, and the UV emission almost seems anti-correlated to the H_2 emission. Complex physical effects are clearly at work in this region. We return to this issue in Section 4.2.

4. Discussion

4.1. Entrainment of H_2

The total amount of warm H_2 gas entrained in the wind of M82 may be estimated from the luminosity of H_2 2.12 μm outside the disk. For this, we follow the calculations of Scoville et al. (1982) which assume that the H_2 molecules are thermalized at T = 2000 K. The resulting prescription is $M_{H_2} = 0.00133\ [L_{S(1)}/L_\odot]\ M_\odot$. From our data, we find that $M_{H_2} \sim 5000\ M_\odot$ (NW) + 7000 $M_\odot$ (SE) = $1.2 \times 10^4 M_\odot$ is located outside the central 5 × 1 kpc region. This represents less than $\sim 10^{-4}$ of the mass of outflowing cold molecular material detected by Walter et al. (2002; $\sim 4 \times 10^8 M_\odot$). Assuming the warm H_2 material shares the same kinematics as the cold molecular material, the total kinetic energy of the warm H_2 material $\sim M_{H_2} v^2_{\rm H2-outflow} \sim 10^{51} \times (v_{\rm H2-outflow}/v_{\rm CO-outflow})^2$ ergs, where $v_{\rm H2-outflow}$ is the average H_2 outflow velocity and $v_{\rm CO-outflow} \sim 100$ km s^{-1}, the average deprojected CO outflow velocity derived by Walter et al. (2002). This is four orders of magnitudes lower than the kinetic energies of the entrained ionized Hα-emitting gas (Shopbell & Bland-Hawthorn 1998, $\sim 2 \times 10^{55}$ ergs) and molecular CO-emitting material (Walter et al. 2002, $\sim 3 \times 10^{55}$ ergs). The warm H_2 material is therefore not a dynamically important component of the outflow.

The detailed processes by which the disk ISM is entrained in the wind without destroying the molecular gas and mass-loading the wind in the process are not well understood. The mere presence of molecular material ∼3 kpc from the disk provides strong constraints on the stability of wind-entrained clouds against photo- and thermal-evaporation, Kelvin-Helmoltz instabilities, and shedding events due to ablation (e.g. Marcolini et al. 2005). The time scale to bring such clouds out to a distance of 3 kpc is $\sim 10^7\ (v_{\rm H2-outflow}/v_{\rm CO-outflow})^{-1}$ yrs, assuming they entered the wind near the center. Recent high resolution three-dimensional simulations of a non-uniform (fractal) radiative cloud in a supersonic flow show that radiative cooling indeed helps stabilize the cloud against disruption over a long enough time scale to allow the cloud to reach velocities in excess of ~ 100 km s^{-1}, but it is not clear that the cloud can survive for as long as $\sim 10^7$ yrs in the flow (Cooper et al. 2009).

Numerical simulations tailored to the wind of M82 (Cooper et al. 2008) show that the original distribution of the inhomogeneous ISM in the disk is important in determining the overall morphology of the wind, as well as the distribution of the entrained filaments. The filled-in structures observed in the fractal ISM simulations of Cooper et al. (2008) shares a greater resemblance with the complex filamentary topology of the H_2 emission than the sharp-edge quasi-conical structures derived from Hα (McKeith et al. 1995; Shopbell & Bland-Hawthorn 1998; cf. Westmoquette et al. 2007, 2009). The dense molecular medium probed by H_2 2.12 μm thus keeps a stronger imprint of the multi-phase, cloudy ISM originally in the disk than the ionized Hα- and X-ray-emitting medium, which likely represents material that has broken up from the denser clouds and has been accelerated further by the wind.

4.2. Excitation and Heating of Extraplanar H_2

There is a vast literature on the dense molecular gas in the disk of M82. Molecular line studies indicate that the intense UV radiation field from the starburst (large G_0 in the nomenclature of Tielens & Hollenbach 1985) has a strong influence on the physical conditions, of the disk material (e.g. Lord et al. 1996; Mao et al. 2000; Fuente et al. 2008; cf. Spaans & Meijerink 2007 for a discussion of the effects of X-rays). The near-infrared rovibrational H_2 emission lines are produced in these PDRs (or XDRs, X-ray dominated regions, in Spaans & Meijerink 2007).

There are two basic ways to excite molecular hydrogen: collisional excitation, i.e. inelastic collisions between molecules in a warm gas ($>$ 1000 K), or fluorescent excitation ("UV pumping") through absorption of soft-UV radiation (912 – 1108 Å) in the Lyman and Werner bands. The latter dominates if G_0/n is large (n is the hydrogen density in the PDR). The method most commonly used to differentiate between collisional excitation from fluorescence consists in using flux ratios of various rovibrational H_2 lines visible in the K band, particularly H_2 $v = 1{-}0$ S(1) 2.12125 μm and the weaker $v = 1{-}0$ S(0) 2.2227 μm and $v = 2{-}1$ S(1) 2.2471 μm transitions. Results have favored thermal excitation of H_2 and ruled out any significant radiative fluorescent contribution in the *cores* of most starburst galaxies, including M82 (e.g. Moorwood & Oliva 1990; Förster Schreiber et al. 2001 and references therein). The UV flux seen by the halo material of M82 is necessarily lower than in the nucleus, but the density of this material is probably also lower than in the disk, so a significant contribution from UV excitation cannot be formally ruled out in the extraplanar H_2 of M82.

In the alternative scenario of collisional excitation, three mechanisms may provide the heating: (1) UV radiation from the starburst, (2) X-rays from the starburst and wind, or (3)

shocks induced by the outflow. A strong constraint on the importance of UV heating can be derived from the ratios of H_2 2.12 μm to Hα (or, equivalently, Brγ; e.g. Puxley et al. 1990; Doyon et al. 1994), while the relative H_2 1−0 S(1) and X-ray fluxes provide an excellent way to test the mechanism of X-ray heating (e.g. Veilleux et al. 1997). The third and final scenario may be tested using shock diagnostics. The lack of one-to-one match between the radial streamers seen near the disk in H_2 (Figure 3, middle) and the shock-heated [Fe II] and SiO filaments of Alonso-Herrero et al. (2003) and García-Burillo et al. (2001) favors UV excitation/heating or X-ray heating over shock heating in this region. The fact that the brightest H_2 emission in the SE extension is fairly well correlated with the "inverted" ionization cone seen in the [N II]/Hα ratio map of M82 suggests that UV excitation/heating is important there, since this is a region where photoionization by OB stars dominates over shocks (Shopbell & Bland-Hawthorn 1998). One also expects a loose correlation between H_2 and PAH emission in this region since the latter is due to transient heating by individual near-UV (< 13.6 eV) photons; this is confirmed in Figure 3 (bottom panels).

Outside this region, shocks are believed to be relatively more important at producing the bright Hα filaments (large [N II]/Hα ratios are observed there; Shopbell & Bland-Hawthorn 1998). This may explain the larger H_2-to-PAH ratios there (enhanced H_2 emission from shock heating) and generally weaker correspondence between H_2, PAH, and Hα features (Hα emission requires energetic > 13.6 eV photons or shocks which are capable of destroying H_2 and macromolecules like PAHs; e.g. Reach et al. 2006). However, this explanation is clearly not valid in the fainter, more diffuse, PAH-emitting material since it is not detected in Hα and barely visible in H_2. The data do not allow us to determine whether the conditions in this gas favor higher UV photodissociation of H_2 (e.g. lower H_2 self-shielding due to broader lines), higher near-UV heating of PAHs, or lower H_2 formation rates on grains (e.g. lower density gas, higher grain processing, or lower sticking coefficient in warm gas; Wolfire et al. 2008 and references therein).

5. Concluding Remarks

We have shown that deep H_2 2.12 μm observations are an excellent complement to mid-infrared PAH and mm-wave CO observations in the search and analysis of the dusty molecular component in the winds of nearby galaxies. Our deep H_2 2.12 μm image of M82 reveals a complex of knots and filaments that extends more than $\sim$3 kpc above and below the disk plane in the same general direction as the well-known galactic wind in this system. This warm molecular material is not a dynamically important component of the outflow, but it is potentially a sensitive tracer of the cooler, more dominant, molecular wind-entrained

material. Detailed morphological comparisons with published data at other wavelengths reveal the complex, multi-phase nature of the wind-entrained material. The results favor UV excitation/heating (shock heating) as the principal H_2 emission process in the inner (outer) bright filaments of the wind, but other processes are probably at work in the fainter, more diffuse, PAH-emitting material where the H_2 emission is apparently suppressed relative to the PAHs. On-going and planned infrared spectroscopy of M82 by various groups should soon be able to test these results and better quantify the energetics, hence impact, of the molecular wind on the large-scale environment of M82.

Support for this work was provided to S.V. and D.S.N.R. by NSF through contract AST 0606932. S.V. also acknowledges support from a Senior Award from the Alexander von Humboldt Foundation and thanks the host institution, MPE Garching, where this paper was written. The authors are grateful to Ron Probst and the rest of the NEWFIRM team for putting together such an outstanding instrument, and to Frank Valdes and Tracy Huard for their assistance with the NEWFIRM Science Pipeline. The authors thank David Fanning for the expert advice and software dealing with images in IDL, provided at `www.dfanning.com`, and Mark Wolfire and the referee for a critical reading of the manuscript and for making some key suggestions which improved the paper. This work has made use of NASA/ADS Abstract Service and the NASA/IPAC Extragalactic Database (NED), which is operated by JPL/Caltech, under contract with NASA.

REFERENCES

Alonso-Herrero, A., et al. 2003, AJ, 125, 1210

Alton, P. B., Davies, J. I., & Bianchi, S. 1999, A&A, 343, 51

Bland-Hawthorn, J., & Cohen, M. 2003, ApJ, 582, 246

Cecil, G., Bland-Hawthorn, J., Veilleux, S., & Filippenko, A. V. 2001, ApJ, 555, 338

Cooper, J., Bicknell, G., Sutherland, R., & Bland-Hawthorn, J. 2008, ApJ, 674, 157

Cooper, J., Bicknell, G., Sutherland, R., & Bland-Hawthorn, J. 2009, ApJ, submitted

Devine, D., & Bally, J. 1999, ApJ, 510, 197

Doyon, R., Puxley, P. J., & Joseph, R. D. 1994, ApJ, 421, 115

Engelbracht, C. W., et al. 2006, ApJ, 642, L127

Förster Schreiber, N. M, et al. 2001, ApJ, 552, 544

Fowler, A. M., & Gatley, I. 1990, ApJ, 353, L33

Fuente, A., et al. 2008, A&A, 492, 675

García-Burillo, S., Martín-Pintado, J., & Fuente, A. 2001, ApJ, 563, L27

Hoopes, C. G., et al. 2005, ApJ, 619, L99

Howk, J. C. 2009, preprint (astro-ph/0904.4928)

Hughes, D. H., Gear, W. K., & Robson, E. I. 1994, MNRAS, 270, 641

Karachentsev, I. D., et al. 2002, A&A, 383, 125

Lehnert, M. D., Heckman, T. M., & Weaver, K. A. 1999, ApJ, 523, 575-584

Loiseau, N., et al. 1990, A&A, 228, 331

Lord, S. D., et al. 1996, ApJ, 465, 703

Lupton, R. H., Gunn, J. E., & Szalay, A. S. 1999, AJ, 118, 1406

Mao, R. Q., et al. 2000, A&A, 358, 433

Marcolini, A., et al. 2005, MNRAS, 362, 626

Martin, C. L. 2006, ApJ, 647, 222

McKeith, C. D., et al. 1995, A&A, 293, 703

Moorwood, A. F. M., & Oliva, E. 1990, A&A, 239, 78

Mutchler, M., et al. 2007, PASP, 119, 1

Nakai, N., et al. 1987, PASJ, 39, 685

Phillips, A. C. 1993, AJ, 105, 486

Probst, R. G., et al. 2008, SPIE, 7014, 93

Puxley, P. J., Hawarden, T. G., & Mountain, C. M. 1990, ApJ, 364, 77

Radovich, M., Kahanpää, J., & Lemke, D. 2001, A&A, 377, 73

Reach, W. T., Rho, J., Jarrett, T. H., & Lagage, P.-O. 2002, ApJ, 564, 302

Reach, W. T., et al. 2006, AJ, 131, 1479

Rupke, D. S., Veilleux, S., & Sanders, D. B. 2005a, ApJS, 160, 87

———. 2005b, ApJS, 160, 115

Shopbell, P. L., & Bland-Hawthorn, J. 1998, ApJ, 493, 129

Spaans, M., & Meijerink, R. 2007, ApJ, 664, L23

Stevens, I. R., Read, A. M., & Bravo-Guerrero, J. 2003, MNRAS, 343, L47

Strickland, D. K., & Heckman, T. M. 2009, ApJ, in press (astro-ph/0903.4175)

Strickland, D. K., & Stevens, I. R. 2000, MNRAS, 314, 511

Swaters, R. A., Valdes, F., & Dickinson, M. E. 2009, preprint (astro-ph/0902.1458)

Tielens, A. G. G. M., & Hollenbach, D. 1985, ApJ, 291, 722

Veilleux, S., Cecil, G., & Bland-Hawthorn, J. 2005, ARA&A, 43, 769

Veilleux, S., Goodrich, R. W., & Hill, G. J. 1997, ApJ, 477, 631

Veilleux, S., Kim, D.-C., Sanders, D. B., Mazzarella, J. M., & Soifer, B. T. 1995, ApJS, 98, 171

Walter, F., Weiss, A., & Scoville, N. 2002, ApJ, 580, L21

Westmoquette, M. S., et al. 2007, ApJ, 671, 358

Westmoquette, M. S., et al. 2009, ApJ, 696, 192

Wolfire, M. G., Tielens, A. G. G. M., Hollenbach, D., & Kaufman, M. J. 2008, ApJ, 680, 384

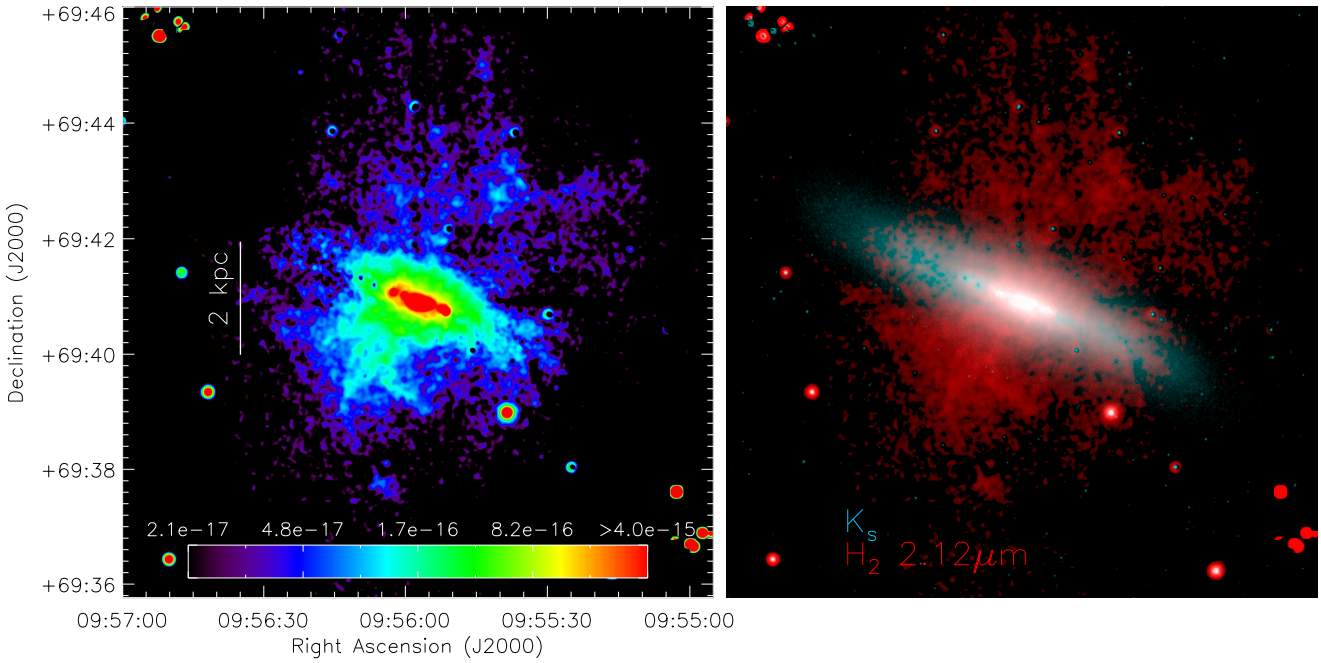

Fig. 1.— H_2 2.12 μm emission in M82. (*left*) "Pure" H_2 emission on a false-color scale. (*right*) H_2 (red) + K_s continuum (blue) emission. The H_2 data were continuum subtracted and smoothed with a 4″ Gaussian kernel to bring out the large scale structure. The intensity scalings in this figure are "asinh" from Lupton et al. (1999). The flux scale is in ergs s^{-1} cm^{-2} $arcsec^{-2}$.

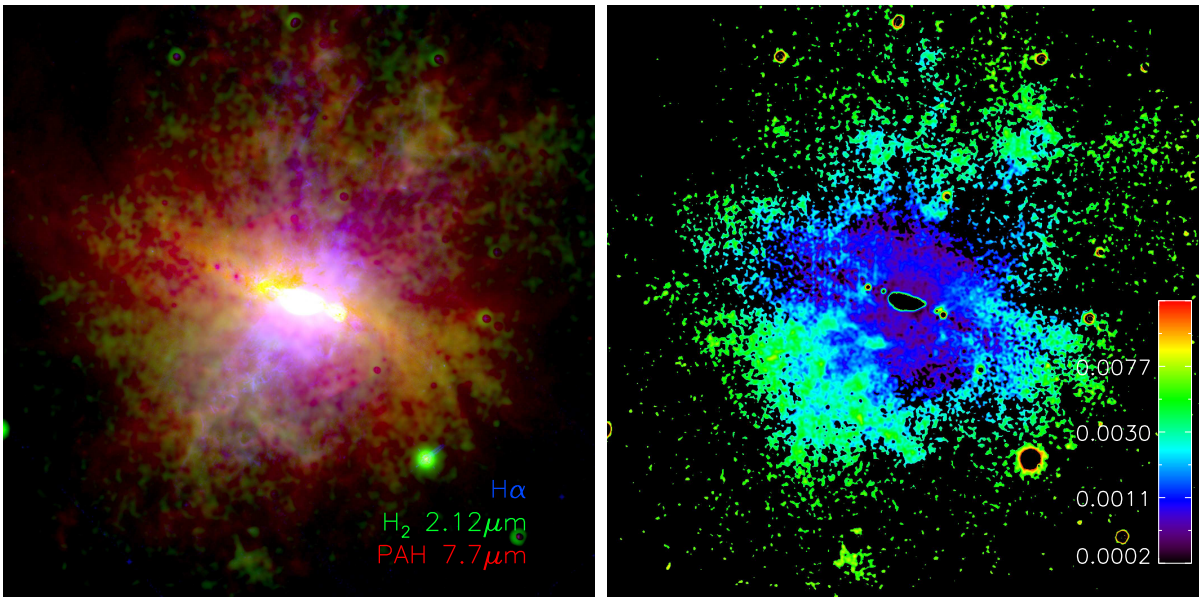

Fig. 2.— (*left*) Three-color composite of M82: *Green:* H_2 2.12 μ emission (same as Figure 1), *Red:* 7.7 + 8.6 μm PAH emission from Engelbracht et al. (2006), and *Blue: HST*/ACS continuum-subtracted Hα emission from Mutchler et al. (2007), smoothed to 0.″2. See Figure 1 for information on intensity scaling. (*right*) H_2-to-PAH emisssion ratio map in the brightest H_2 filaments. Black regions are of low S/N or affected by saturation effects. The absolute ratio scale is accurate to within a factor of only ∼2 due to PSF mismatch between the two wavebands, lack of color corrections for the IRAC photometry, and stellar contamination to the 8 μm flux.

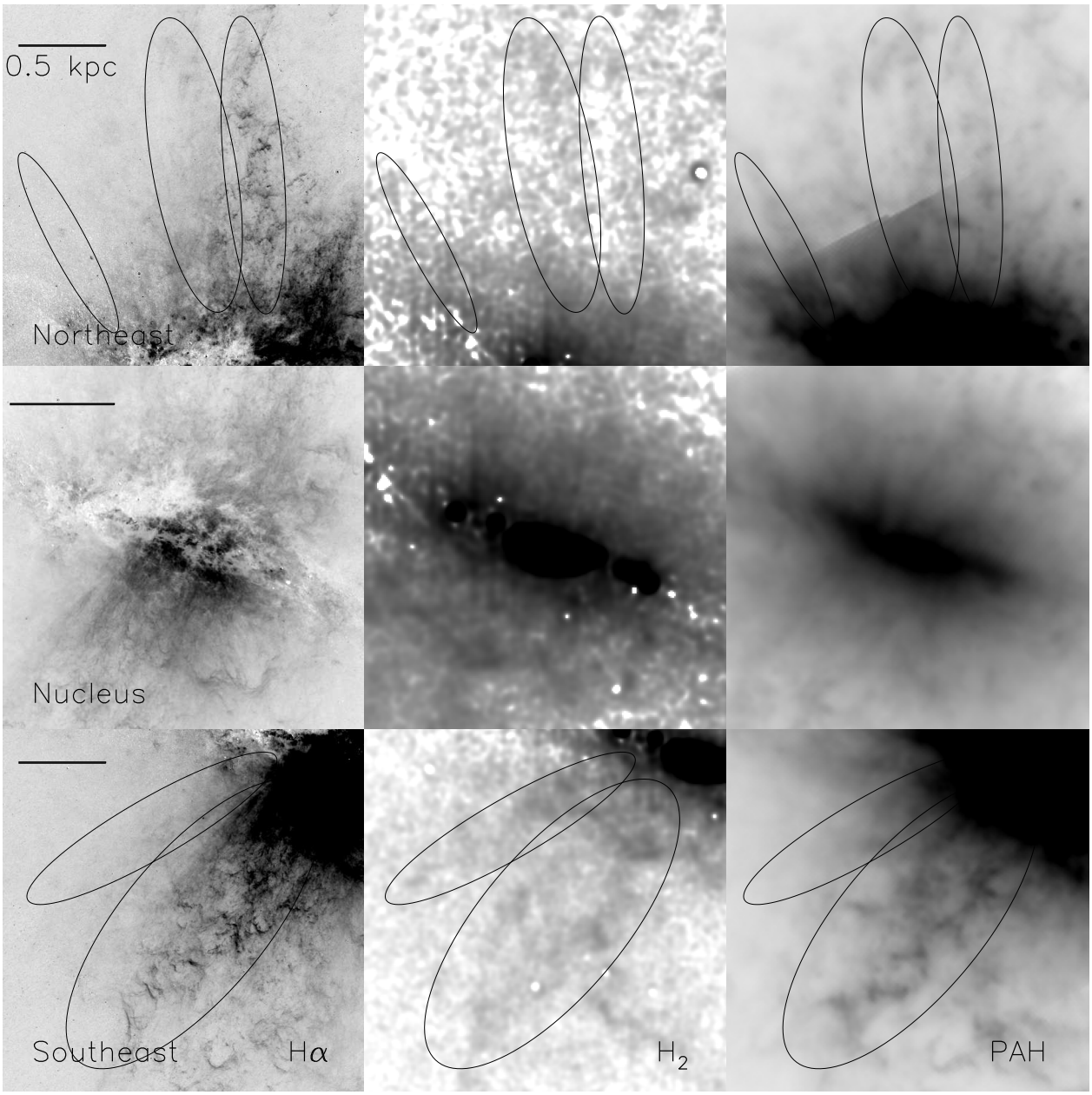

Fig. 3.— Large-scale images (2′ wide) that focus on three regions of coherent H_2 2.12 μm emission (central column; smoothed with 4″ Gaussian kernel) and compare with the Hα (left; 0.″2) and PAH (right) emission. Shown in the top, middle, and bottom rows are the NE quadrant, nuclear disk region, and SE quadrant, respectively. See Figure 1 for information on intensity scaling. The ellipses delineate prominent radial filaments that appear in at least one waveband.

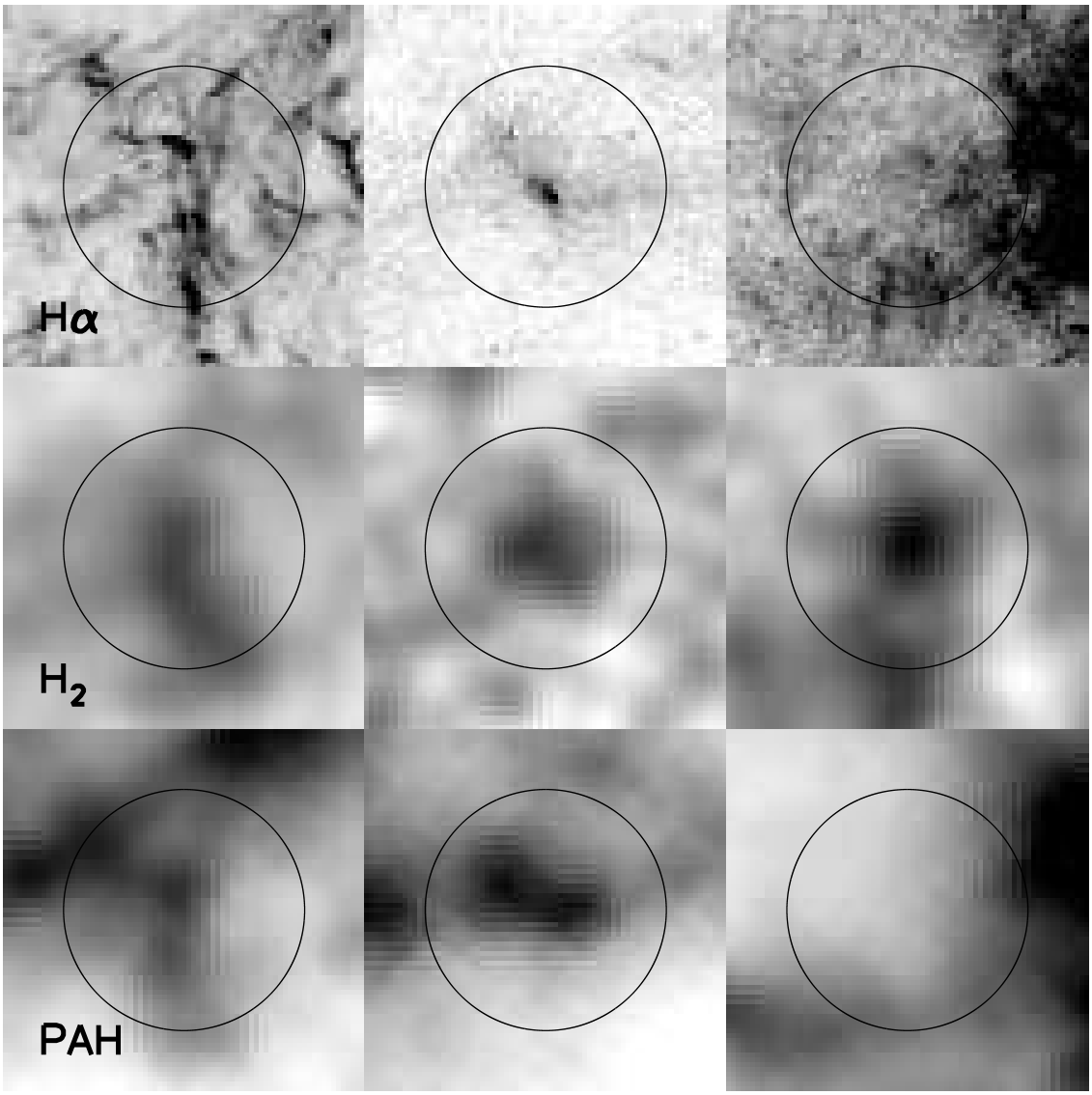

Fig. 4.— Examples of small-scale features in H_2 2.12 μm (middle row; 2″ Gaussian kernel), Hα (top row; 0.″2.) and PAH (bottom row) emission. See Figure 1 for information on intensity scaling. The circles are 10″ in diameter.